ChemComm
Chemical Communications

Accepted Manuscript

This article can be cited before page numbers have been issued, to do this please use: H. Gong, Y. Wu, R. Zeng, Y. Zeng, X. Liu and D. Tang, *Chem. Commun.*, 2021, DOI: 10.1039/D1CC03743A.

ROYAL SOCIETY OF CHEMISTRY

rsc.li/chemcomm

View Article Online
DOI: 10.1039/D1CC03743A

Journal Name

COMMUNICATION

CRISPR/Cas12a-mediated liposome-amplified strategy for photoelectrochemical detection of nucleic acid†

Hexiang Gong,[a] Yulin Wu,[a] Ruijin Zeng,[a] Yongyi Zeng,[b] Xiaolong Liu[b,*] and Dianping Tang[a,*]

Received 00th January 20xx,
Accepted 00th January 20xx

DOI: 10.1039/x0xx00000x

www.rsc.org/

This work reports a photoelectrochemical biosensor for dopamine-loaded liposome-encoded magnetic beads cleaved by clustered regularly interspaced short palindromic repeats (CRISPR)/Cas 12a system for quantification of human papillomavirus (HPV)-related DNA by using neodymium-doped BiOBr nanosheets (Nd-BiOBr) as photoactive matrix. Magnetic beads and dopamine-loaded liposomes are covalently attached to both ends of ssDNA to construct dumbbell-shaped dopamine-loaded liposome-encoded magnetic beads (DLL-MB) probes. When the guide RNA binds to the target HPV-16, the ssDNA will be cleaved by Cas12a, thereby degrading the double dumbbell probes. After magnetic separation, the dissolved DLL are treated with Triton X-100 to release the dopamine (as an electron donor), which was then detected as an amplified photocurrent on the Nd-BiOBr-based photoelectrode.

Photoelectrochemical (PEC) DNA biosensor, as a newly emerged and popular sensing technique, is developed by fusion of photoactive semiconductors and nucleic acid signal amplification technology, and has attracted great attention due to its functions of high sensitivity, low background noise and easy miniaturization.[1-3] Until now, diverse innovative PEC DNA schemes have been reported for the detection of small molecules, various types of nucleic acid fragments, tumor markers, enzymes activity, cells, and so forth.[4-6] For instance, Zeng *et al*. devised some newly nucleic acid signal amplification/DNA polymer techniques in PEC DNA biosensor for the detection of small molecules, including palindromic fragment-mediated single-chain amplification, branched hybridization chain reaction, DNA flowers and DNA hydrogel.[7-10] Despite great progress has been made, PEC sensing still faces the insufficiency of distortion and high background in the process of nucleic acid signal amplification. For example, non-enzyme reactions (branched hybridization chain reaction) may produce false positive signals, while enzyme-mediated reactions often have many side reactions, making it difficult to achieve the pre-designed effect. Therefore, exploring simple nucleic acid signal amplification and ease of operation without affecting sensitivity and versatility is a good strategy for solving current PEC biosensing.

Clustered regularly interspaced short palindromic repeats (CRISPR)/Cas system that guide RNA directs the CRISPR-associated proteins (Cas) to desire nucleic acid fragments to activate Cas nuclease activity, not only set off in molecular biology but also caused the innovation of biological analysis and molecular diagnostic technology.[11-14] The advantage of this technology lies in the trans cleavage activity of the Cas enzyme (such as Cas12a), which can efficiently degrade ssDNA reporters (thousands of turnovers per second), so the detection sensitivity can be significantly improved.[15-19] More notably, compared with other enzyme-mediated nucleic acid signal amplification technologies, the CRISPR/Cas system maintains high efficiency during the execution of the CRISPR/Cas system without cumbersome primer design and excessively harsh experimental operations. Recently, our laboratory reported a CRISPR/Cas12a-based piezoresistive platform for the ultrasensitive and simple detection of nucleic acid by using $Ti_3C_2T_x$-PEDOT:PSS/PDMS as signal transduction intermediary.[20] It is expected that the introduction of CRISPR/Cas12a technology into PEC DNA biosensors is an important supplement to traditional DNA signal amplification.

Motivated by these pioneering works, herein, this study designs an advanced and feasible CRISPR/Cas12a-based PEC technology for the detection of human papillomavirus 16 (HPV-16). Dopamine-loaded liposome-encoded magnetic beads (DLL-MB) are connected by a short strand of ssDNA and serve as substrate for CRISPR/Cas12a digestion. When the target HPV-16 DNA is present, with the assistance of the Cas12a-crRNA system, the resulting Cas12a-crRNA-HPV-16 is activated and has

[a] *Key Laboratory for Analytical Science of Food Safety and Biology (MOE & Fujian Province), State Key Laboratory of Photocatalysis on Energy and Environment, Department of Chemistry, Fuzhou University, Fuzhou 350108, China. E-mail: dianping.tang@fzu.edu.cn (D. Tang)*
[b] *The United Innovation of Mengchao Hepatobiliary Technology Key Laboratory of Fujian Province, Mengchao Hepatobiliary Hospital of Fujian Medical University, Fuzhou 350025, China. E-mail: xiaoloong.liu@gmail.com (X. Liu)*
† *Electronic Supplementary Information (ESI) available: See DOI: 10.1039/x0xx00000x*

the ability to cleave the ssDNA in the DLL-MB, so that the dopamine-loaded liposomes are separated from the surface of magnetic beads. The separated dopamine-loaded liposomes can release dopamine after lysis, which can significantly enhance the photocurrent of Nd-BiOBr nanosheets. In this sensing system, a trace amount of target HPV-16 can be converted to numerous dopamine molecules, leading to a remarkable amplification photocurrent of Nd-BiOBr via CRISPR/Cas12a and the liposome-encoded enzyme catalytic. In this contribution, we make full use of the characteristics of the CRISPR/Cas12a signal amplification mode, and endow a new concept of developing an advanced PEC DNA biosensor to screen biomolecules.

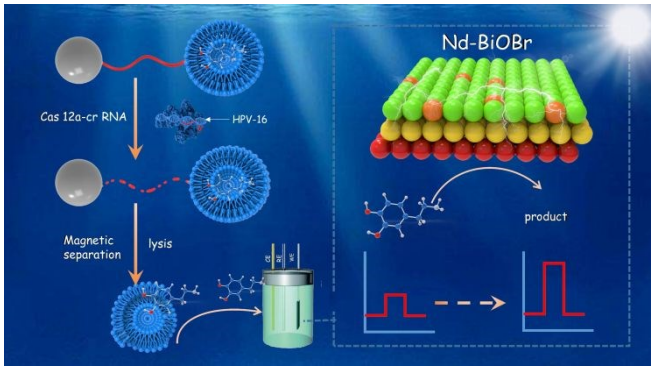

Scheme 1 Schematic illustration of the photoelectrochemical biosensor toward human papillomavirus 16 (HPV-16)-related DNA on dumbbell-shaped dopamine-loaded liposome-encoded magnetic beads (DLL-MB) probes based on CRISPR/Cas12a signal amplification, by using neodymium-doped BiOBr nanosheets (Nd-BiOBr) as photoactive matrix.

The intrinsic morphology of the as-synthesized Nd-BiOBr was characterized by using scanning electron microscopy (SEM; Fig. 1A) and transmission electron microscopy (TEM; Fig. 1B). TEM and SEM images together showed that the prepared Nd-BiOBr had different sizes with a square-like nanostructure. To testify the elemental composition of Nd-BiOBr, energy-dispersive X-ray (EDX) elemental mapping analysis (Fig. S1) was carried out. A relatively smooth and regular flake structure was observed in the high-angle circular dark-field scanning transmission electron microscope (HAADF-STEM, Fig. 1C) image. The corresponding element mappings (Fig. 1D) on the scanning area proved the coexistence and homogeneous dispersion of Br, O, Bi, and Nd elements in the entire composite, indicating that Nd element is successfully incorporated into BiOBr. The XRD peaks (Fig. 1E) determined for the Nd-BiOBr could be assigned to tetragonal BiOBr (JCPDS file 09-0393) without any impurity peaks, suggesting good crystalline quality of the synthesized samples. However, no diffraction peaks belonging to Nd products were detected in the Nd-BiOBr nanocomposite, which may be due to relatively low element content or crystal quality. To gain insight into the atomic valence state and electronic interaction, X-ray photoelectron spectroscopy (XPS; the calibrated carbon peak at 284.8 eV) was further checked. As shown from XPS survey spectrum in Fig. 1F, all element valences (Nd 3d; O 1s; Bi 4f and Br 3d) could be observed in Nd-BiOBr. The binding energies of Br $3d_{5/2}$ and Br $3d_{3/2}$ were 68.15 eV and 69.40 eV (Fig. 1G), which could attribute to the Br^- species existing in the composites.[21] Meanwhile, the Nd 3d of the Nd-BiOBr also presented the characteristic double signals at 981.75 eV (Nd $3d_{5/2}$) and 1005.00 eV (Nd $3d_{3/2}$), confirming the existence of Nd^{3+} state (inset in Fig. 1G).[22] Besides, the O 1s peak was reasonably fitted with two component peaks located at 530.30 eV and 532.65 eV (Fig. 1H), corresponding to crystal lattice O atoms (Bi-O, BiOBr) and surface hydroxyl groups, respectively.[23] Similarly, the spin-orbit components of two individual peaks situated at 158.95 eV and 164.15 eV (Fig. 1I), corresponding to Bi^{3+} $4f_{7/2}$ and Bi^{3+} $4f_{5/2}$ in Nd-BiOBr, respectively.[24]

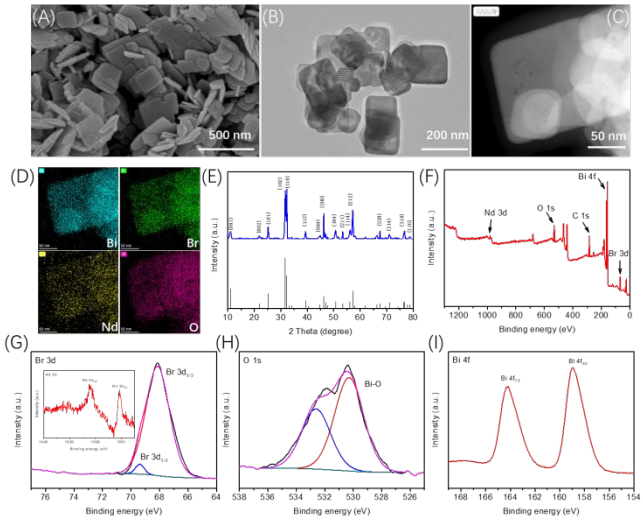

Fig. 1 (A) SEM image, (B) TEM image, (C) HAADF-STEM image, (D) element mappings, (E) XRD pattern and (F) XPS survey spectrum of Nd-BiOBr; high-resolution XPS spectra of (G) Br 3d, Nd 3d (inset in G), (H) O 1s and (I) Bi 4f.

In our design, the next two inevitable questions arise as (i) whether the Nd-BiOBr nanomaterials have photocurrent response to dopamine, and (ii) whether the CRISPR/Cas12a signal amplification technology can perform as expected. To verify the above assumptions, we next designed a series of control experiments to prove the feasibility of the program. As the concentration of dopamine gradually increases, the photocurrent based on Nd-BiOBr/FTO gradually increases and presents a good linear relationship (I (nA) = 15.31 × $C_{[dopamine]}$ + 137.2 (μM), R^2 = 0.9623, Fig. 2A-B). The improved photocurrent response can be attributed to the role of dopamine as a good electron donor. The HPV-16 activation of CRISPR/Cas12a cleavage activity was first verified by native polyacrylamide gel electrophoresis (PAGE, 20%, Fig. 2C) using random ssDNA as the nonspecific substrate. Lanes 'a' and 'b' represent random DNA and HPV-16, respectively, and can coexist in lane 'c'. Furthermore, Cas 12a and crRNA were added to the reaction solution in lane 'c', and it was found that the band located at random DNA position disappeared (lane 'd'). PAGE results preliminarily indicate that Cas12a-crRNA-HPV-16 triplex assembly can successfully activate the cleavage activity of

ssDNA. To further confirm the above results, a fluorescent effect was performed in a confocal laser scanning microscope to illustrate the effect of CRISPR/Cas12a enzyme digestion, and MB-ssDNA-FAM was used as a fluorescent digestion substrate. In our design, biotin/FAM modified long ssDNA was attached to the surface of streptavidin-modified MB to obtain MB-ssDNA-FAM. Once the ssDNA digestion activity of Cas12a-crRNA is activated by the analyte, the ssDNA on the surface of MB-ssDNA-FAM will be degraded to a certain extent and the fluorescence will change. Comparing with (Fig. 2D) or without (Fig. 2E) the analyte HPV-16, we can find a significant change in the fluorescence of MB-ssDNA-FAM. Significantly, only in the presence of the analyte HPV-16, almost no fluorescent signal is observed, indicating that HPV-16 can well activate the enzyme cleavage of Cas12a. Then we replaced dopamine-loaded liposome with FAM to construct dopamine-loaded liposome-encoded magnetic beads (DLL-MB). To investigate the successful preparation of DLL, negative-stain TEM was utilized to characterize its morphological characteristics. Fig. 2F shows that the NS-TEM image of the DLL exhibited a spherical or quasi-spherical shape with clear edges. The dynamic light scattering (DLS) measurement in Fig. 2G shows that the range of DLL diameters spanned 35-155 nm (the average diameter: 76.95 nm), and the polydispersity index was 0.166. Moreover, atomic force microscopy image in Fig. 2H illustrates that DLL were well dispersed with spherical shape, which agrees quite well with the TEM data. Finally, we used dopamine-loaded liposome-encoded magnetic beads (DLL-MB) probes and CRISPR/Cas12a to verify the feasibility (Fig. 2I). Remarkably, the photocurrent obtained by the reaction solution in the absence of analyte was not significantly different from the Nd-BiOBr/FTO photocurrent (curve a vs curve b). When 100 nM HPV-16 was present in the solution, the photocurrent increased sharply. These results further revealed that our developed DLL-MB probes and CRISPR/Cas12a system could be utilized for detection of HPV-16.

To evaluate the analytical performance and quantitative range of the CRISPR/Cas12a-based PEC biosensor, different-level of HPV-16 were determined under optimized conditions. In Fig. 3A, as the concentration of the target grew, the photocurrent intensity also increased dynamically due to the increased amount of released electron donor dopamine resulting from the increased amount of activated CRISPR-Cas 12a complex. Favorably, a preferable linear-dependence photocurrent-logarithm of HPV-16 concentration curve was acquired, and the corresponding regression equation was I (nA) = 42.13 × $\log C_{[HPV-16]}$ + 308.25 (nM) with high reliability (R^2 = 0.9876, n = 6) (Fig. 3B). The detection limit (LOD) was as low as 1.6 pM at a signal-to-noise ratio of 3. Moreover, the linear range and LOD were acceptable, as compared with CRISPR/Cas12a-powered biosensors and other existing HPV-16 detection strategies (Table S1).

The specificity of the designed PEC biosensor for HPV-16 assay is demonstrated by using another high-risk HPV genotype (HPV-18) as an interfering substance under the same conditions. As depicted in Fig. 3C, compared with the blank sample (PBS), the photocurrent response induced by the addition of HPV-18 analogues was largely negligible, while in the mixture of HPV-16 and HPV-18, only current values similar to those of HPV-16 alone were presented, revealing the CRISPR/Cas12a with excellent specificity. Besides, the relative standard deviations (RSDs) of using the within-batch (intra-assay) were 3.25%, 4.11%, and 4.03%, whereas those of using the various-batch (inter-assay) were 6.17%, 8.27%, and 7.14% (*n* = 3) toward the 0.005 nM, 5.0 nM, and 50 nM HPV-16, respectively, undoubtedly demonstrating good precision and reproducibility.

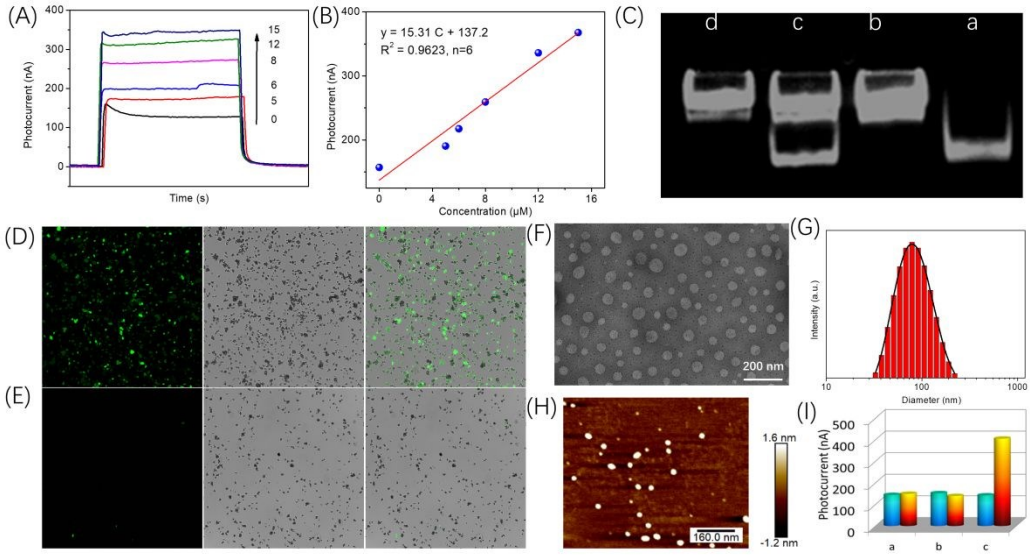

Fig. 2 (A) Photocurrents curves of the Nd-BiOBr/FTO after incubated with dopamine standards including 0, 5, 6, 8, 12, and 15 μM; and (B) the calibration curve corresponding to the photocurrents as a function of dopamine concentration. (C) PAGE results for different samples: lane 'a': 500 nM random DNA as the substrate; lane 'b': 500 nM HPV-16; lane 'c': 500 nM HPV-16 + 500 nM random DNA; lane 'd': 500 nM HPV-16 + 500 nM random DNA + crRNA+ Cas 12a; confocal fluorescence images of samples: (D) MB-ssDNA-FAM + crRNA + Cas 12a and (E) 500 nM HPV-16 +MB-ssDNA-FAM + crRNA + Cas 12a; (F) TEM image, (G) DLS data and (H) AFM image of DLL; (I) photocurrents of (a) Nd-BiOBr/FTO

and (b) Nd-BiOBr/FTO + crRNA + Cas 12a + DLL-MB and (c) Nd-BiOBr/FTO + 100 nM HPV-16 + crRNA + Cas 12a + DLL-MB (blue and orange columns indicate absence or presence of 1% Triton X-100).

View Article Online
DOI: 10.1039/D1CC03743A

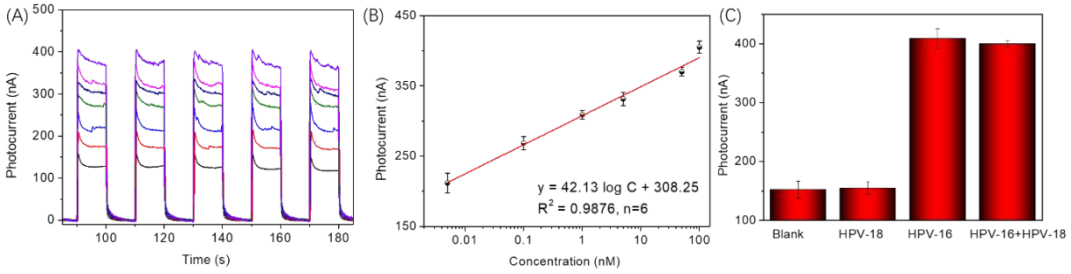

Fig. 3 (A) Dose responses (photocurrents density vs. HPV-16 concentration) of CRISPR/Cas12a-based Nd-BiOBr bioanalysis platform toward target including 0, 0.005, 0.1, 1, 5, 50 and 100 nM; (B) calibration plots between photocurrent (nA) and the logarithm of HPV-16 concentration (nM); and (C) the anti-interference ability against blank (PBS), 100 nM HPV-18, 100 nM HPV-16 and the mixture (100 nM HPV-16 + 100 nM HPV-18).

In summary, this work successfully devised an advanced Nd-BiOBr-based PEC platform for determination of HPV-16 coupling with dopamine-loaded liposomes and trans-cleavage activity of CRISPR/Cas12a system for the signal amplification. Compared with traditional signal amplification strategies, the established analytical platform can overcome problems, *e.g.*, false positives and complex redundant operation by using CRISPR/Cas12a system. Moreover, since liposomes are loaded with a large number of electron donors, which can boost the intensity of photocurrents, a trace amount of target will be detected. Considering the high-efficiency and multifunction of the gene editing-mediated signal amplification mode, the concept of CRISPR/Cas 12a PEC mode opens up new prospects for the early diagnosis of various diseases.

Authors acknowledge financial support from the National Natural Science Foundation of China (21874022 and 21675029).

Conflicts of interest

There are no conflicts to declare.

Notes and references

1. F. Li, S. Wang, H. Yin, Y. Chen, Y. Zhou, J. Huang and S. Ai, *ACS Sen.*, 2020, **5**, 1092-1101.
2. X. Gao, S. Niu, J. Ge, Q. Luan and G. Jie, *Biosens. Bioelectron.*, 2020, **147**, 111778.
3. C. Sui, T. Wang, Y. Zhou, H. Yin, X. Meng, S. Zhang, G. Waterhouse, Q. Xu, Y. Zhuge and S. Ai, *Biosens. Bioelectron.*, 2019, **127**, 38-44.
4. J. Shu and D. Tang, *Chem-Asian J.*, 2017, **12**, 2780-2789.
5. J. Shu and D. Tang, *Anal. Chem.*, 2020, **92**, 363-377.
6. Q. Zhou and D. Tang, *Trends Anal. Chem.*, 2020, **124**, 115814.
7. R. Zeng, Z. Huang, Y. Wang and D. Tang, *Chemelectrochem*, 2020, **7**, 1537-1541.
8. R. Zeng, L. Zhang, Z. Luo and D. Tang, *Anal. Chem.*, 2019, **91**, 7835-7841.
9. R. Zeng, L. Zhang, L. Su, Z. Luo, Q. Zhou and D. Tang, *Biosens. Bioelectron.*, 2019, **133**, 100-106.
10. R. Zeng, Z. Luo, L. Su, L. Zhang, D. Tang, R. Niessner and D. Knopp, *Anal. Chem.*, 2019, **91**, 2447-2454.
11. B. Li, Z. Shao and Y. Chen, *Anal. Chim. Acta.*, 2021, **1165**, 338478.
12. M. Qing, S. Chen, Z. Sun, Y. Fan, H. Luo and N. Li, *Anal. Chem.*, 2021, **93**, 7499-7507.
13. J. Choi, J. Lim, M. Shin, S. Paek and J. Choi, *Nano. Lett.*, 2021, **21**, 693-699.
14. D. Huang, J. Qian, Z. Shi, J. Zhao, M. Fang and Z. Xu, *ACS Synth. Biol.*, 2020, **9**, 3114-3123.
15. O. Mukama, T. Yuan, Z. He, Z. Li, J. Habimana, M. Hussain, W. Li, Z. Yi, Q. Liang and L. Zeng, *Sens. Actuators B Chem.*, 2020, **316**, 128119.
16. F. Li, Q. Ye, M. Chen, B. Zhou, J. Zhang, R. Pang, L. Xue, J. Wang, H. Zeng, S. Wu, Y. Zhang, Y. Ding and Q. Wu, *Biosens. Bioelectron.*, 2021, **179**, 113073.
17. C. Li, B. Zheng, Y. Liu, J. Gao, M. Zheng, D. Pang and H. Tang, *Biosens. Bioelectron.*, 2020, **169**, 112650.
18. B. Li, A. Xia, S. Zhang, T. Suo, Y. Ma, H. Huang, X. Zhang, Y. Chen and X. Zhou, *Biosens. Bioelectron.*, 2021, **173**, 112619.
19. D. Huang, Z. Shi, J. Qian, K. Bi, M. Fang and Z. Xu, *Biotechnol. Bioeng.*, 2021, **118**, 1587-1596.
20. R. Zeng, W. Wang, M. Chen, Q. Wan, C. Wang, D. Knopp and D. Tang, *Nano Energy*, 2021, **82**, 105711.
21. D. Wu, S. Yue, W. Wang, T. An, G. Li, H. Yip, H. Zhao and P. Wong, *Appl. Catal. B Environ.*, 2016, **192**, 35-45.
22. J. Sin, C. Lim, S. Lam, H. Zeng, H. Lin, H. Li and A. Mohamed, *J. Phys. Chem. Solids.*, 2020, **140**, 109382.
23. J. Xia, S. Yin, H. Li, H. Xu, L. Xu and Y. Xu, *Dalton T.*, 2011, **40**, 5249-5258.
24. H. Yu, H. Huang, K. Xu, W. Hao, Y. Guo, S. Wang, X. Shen, S. Pan and Y. Zhang, *ACS Sustain. Chem. Eng.*, 2017, **5**, 10499-10508.